RSC Advances

ROYAL SOCIETY OF CHEMISTRY

www.rsc.org/advances

Ni_3P-Ni arrays electroless deposited on 3-D nickel foam as high performance anode for lithium-ion battery

Shuai Liu[a], Jinkui Feng[a,*], Xiufang Bian[a,*], Jie Liu[b] and Hui Xu[a]

[a] *Key Laboratory for Liquid-Solid Evolution and Processing of Materials (Ministry of Education), School of Materials Science and Engineering, Shandong University, Jinan 250061, China*

[b] *Advanced Fibers &Modern Textile Cultivation Base of State Key Lab, Qingdao University, Qingdao 266071, China*

We prepared advanced Ni_3P-Ni array electrodes for Li-ion battery (LIB) by electroless deposition on 3-D nickel foam successfully. The array structure of Ni_3P-Ni can accommodate volume changes during the lithiation/de-lithiation progress and promote high-rate capability because the interspaces in such structure can act as ideal volume expansion buffers. It shows excellent electrochemical performance as anode material for LIBs.

The search for new electrode materials has become an urgent task in building next generation LIBs, so as to meet the ever-growing requirements for high capacity and high power density[1-5]. Reducing the polarization and enhancing the kinetics in electrode reactions is a promising approach[6, 7]. To that concern, phosphides have attracted much attention due to the low polarization and good cycling stability as promising negative electrodes[8-11]. The charge-discharge polarization ΔV is decreasing as we move from fluorides (about 1.1 V) to oxides (about 0.9 V), sulfides (about 0.7 V), and phosphides (about 0.4 V) [12]. This is fully consistent with the decrease in the M-X bond polarization from M-F to M-P. Therefore, a particular interest comes from the phosphides that react with Li over a narrow potential range. For instance, CoP_3[13] and Cu_3P[14] reversibly react with Li at an average of 1V and show

*Corresponding author. Tel.: +86 531 88392748 E-mail address: jinkui@sdu.edu.cn（Jinkui Feng）
xfbian@sdu.edu.cn (Xiufang Bian)

flat charge and discharge curves separated by about 0.4-0.5V. Additionally, some attempts have been made to improve the capacity retention of the phosphides. The NiP_3 possesses a very promising capacity with a reversible storage capacity higher than 1000 mAh g^{-1} after 50 cycles as negative electrode for LIB[15]. The micro-sized Cu_3P powders obtained by a solvothermal method have the better cycling performance than other Cu_3P powders prepared by ball milling, high temperature[16] or spray method[17, 18]. Nevertheless, it is worth noting that the application of phosphides in practical LIBs is seriously impeded by the relatively large initial irreversible loss and poor capacity retention due to huge volume expansion/contraction during the conversion reaction between lithium ion and phosphides[11, 19, 20]. The repeated processes result in pulverization of the electrodes and finally destroy the initial structure[21]. Additionally, the anode materials with porous structures have exhibited improved cyclic performance because the pores in such structures can act as ideal volume expansion buffers[22]. Similar to porous structure there are also interspaces in array structure. However, the lack of inexpensive and simple methods to mass produce phosphides with array structure limits its use. As a result, it is highly desirable to protect the integrity of the phosphides-based electrodes by rational design taking into account all the above considerations.

The electroless deposition technique of Ni-P alloy coating has been a well known commercial process that has found numerous applications in many fields due to excellent properties of coatings, such as high corrosion resistance, high wear resistance, good lubricity, high hardness, and acceptable ductility[23-25]. We have successfully prepared the Ni-P film and Ni-P composite film[23]. Herein, we report the synthesis and electrochemical properties of Ni_3P-Ni arrays prepared by electroless deposited on 3-D nickel foam. The Ni_3P-Ni arrays exhibits high retention capacity and good rate capability for negative electrodes.

The 3-D nickel foam (purchased from lzy battery sales department in China) with a diameter of 14mm and copper foil (25mm×40mm) (in order to avoid confusion in later analysis) were used as substrates. Specimens were immersed in acetone for 30 min and dried with hair dryer. The plating bath contained 25g L^{-1} $NiSO_4 \cdot 6H_2O$, 25g L^{-1} $NaH_2PO_2 \cdot H_2O$, 12g L^{-1} CH_3COONa, and 28ml L^{-1} lactic acid ($C_3H_6O_3$). Coating deposition took place in a thermostated vessel with a capacity of 200 cm^3 maintained at 80 ^{0}C for 40 min. After the electroless deposition, fresh coatings were annealed at 400 ^{0}C for 1h in vacuum chamber (pressure $< 1\times10^{-3}$ Pa) and naturally cooled with furnace to room temperature. The structure and surface morphology were characterized by X-ray diffraction (XRD, Rigaku Dmaxrc diffractometer) and scanning emission microscope (SEM, Zeiss SUPRA 55), respectively. Electrochemical performance was measured in 2016 coin-type cells. The as-prepared Ni_3P-Ni arrays on 3-D nickel foam was used as the working electrode, Li sheet was used as counter electrode, and Celgard 2400 as the separator, and a mixture of 1M $LiPF_6$ in ethylene carbonate, dimethyl carbonate , diethyl carbonate (1:1:1 by volume) as electrolyte. Half-cells were assembled in a glovebox full of argon (purity >99.99%) with the water and oxygen concentrations below 1 ppm. at room temperature. Galvanostatic discharge/charge cycles were performed between 0.01 and 3 V on a lithium battery cycler (LAND CT-2001A, Wuhan, China). Cyclic voltammetry (CV) was measured by half coin cell on a CHI 660E (Shanghai China) electrochemical workstation.

Fig.1 shows the XRD patterns of the electroless deposited precursor film and annealed film with copper foil as substrate. Copper foil was used as the substrate here (Fig.1a and Fig.1b) in order to avoid confusion in latter analysis. There is only a wide diffraction peak in the precursor film besides the peaks of Cu substrate indicating that the precursor film is amorphous as shown in Fig. 1a. After annealed at 400 ^{0}C for 1h, the film exhibits excellent crystallization (Fig. 1b). It shows the XRD

patterns and EDX (energy-dispersive X-ray) of the electroless deposited film annealed at 400 ^{0}C for 1h. It is clearly seen that all peaks can be well indexed to Ni_3P (JCPDS No. 89-2743) (tetragonal structured) and Ni (JCPDS No.70-0989) (cubic structured). As shown in inset, EDX confirms that the annealed electroless deposited film consists of P and Ni elements. It can be concluded that the annealed electroless deposited film consists of Ni_3P and Ni.

Fig. 2a shows that the surface of uncoated nickel foam substrate (use as current collector) is bare. As shown in Fig. 2d, the corresponding XRD of uncoated Ni foam indicates that the uncoated Ni foam is very pure. The electroless deposited Ni-P coating on Ni foam before annealing is amorphous. After heated at 400 ^{0}C for 1h in vacuum, the coating shows excellent crystallization (composed of Ni_3P phase and Ni phase). The SEM images (Fig. 2b and 2c) of Ni_3P-Ni coating show that the morphology and size distribution of the electroless deposited Ni_3P-Ni arrays are uniform. The array structure can increase the cyclic performance efficiently because the interspaces in such structure can act as ideal volume expansion buffers[21]. The 3-D Ni_3P-Ni coated Ni foam is netlike, as shown in Fig.2e. The nickel foam used as current collector with a three-dimensional network structure not only possesses high electrical conductivity and big surface area, but also it can buffer the large volume change of active materials during lithium insertion and extraction[26]. As shown in Fig. 2f, the EDX mapping of elemental P corresponding to Fig. 2e confirms that the distribution of elemental P is homogeneous on 3-D nickel foam.

The lithium storage performance of Ni_3P-Ni arrays was characterized by cyclic voltammetry (CV) and static-current charge-discharge. Fig. 3a shows CV curves of the Ni_3P-Ni electrode in the 0.01-3 V versus Li/Li^+ potential window at a scan rate of 1 mV s^{-1}. The cathodic peak at the potential of about 1 V can be assigned to the successive phase transformation upon lithium-ion insertion via crystalline

Ni_3P to form Li_3P alloy[9, 10]. During the de-lithiation scan the anodic peak at the potential of about 2.2 V is associated with the re-formation of Ni_3P[27]. The area of reduction peak is almost equal to that of oxidation peak in the first three CV scans, indicating high reversibility and good cycling stability. The Fig. 3b shows the voltage-capacity curves for the Ni_3P-Ni electrode after 1, 10, 20 and 50 cycles at a current density of 0.02 mA cm^{-2} between voltage limits of 0.01-3 V. The voltage profile with different flat plateaus due to the redox reactions associated with Li^+ insertion/extraction could be observed in the first discharge and charge curves. The discharge (Li insertion) and charge (Li extraction) capacities of the Ni_3P-Ni were 913.7 mAh g^{-1} and 395 mAh g^{-1}, respectively, corresponding to a first-cycle efficiency of 43.2 % (as shown in Fig. 3c). The irreversible capacity ratio could be assigned to the decomposition of electrolyte, forming a solid/electrolyte interphase (SEI) on the electrode surface[27, 28], and to the irreversible insertion of Li ions into the Ni_3P-Ni. Moreover, the Ni_3P-Ni arrays exhibited excellent capacity retention and maintained a stable capacity of 360 mAh g^{-1} with a high coulombic efficiency after 100 cycles at a current density of 0.02 mA cm^{-2}. As shown in Fig. 3d, the Ni_3P-Ni arrays were allowed to discharge/charge at higher current densities. Highly stable reversible capacities around 398, 352 and 320 mAh g^{-1} were obtained at current densities of 0.02, 0.04, 0.06 mA cm^{-2}, respectively.

Compared with the morphologies of as-deposited Ni_3P-Ni arrays (Fig. 4a), there is a clear volume expansion of the lithiated arrays (Fig. 4b) after 100 cycles at a current density of 0.02 mA cm^{-2} between voltage limits of 0.01-3 V. The large volume expansion is caused by Li insertion. However, the space between the arrays can accommodate the volume change associated with Li insertion. As shown in the schematic of the lithiation (Fig. 4c pristine and Fig. 4d lithiated), the integrity of the Ni_3P-Ni electrodes can be protected by the array structure during lithiation process. In order to confirm that Li^+ was

actually inserted into the Ni_3P-Ni arrays during cycling, XRD scans were performed on a Ni_3P-Ni film grown on nickel foam substrate before and after charging with Li^+. As shown in Fig. 4e, there is a shift in XRD peak positions. Compared with the Ni_3P (231) peak of the as-deposited electrode, the (231) peak of the lithiated electrode has shifted to higher 2θ angles, indicating a lattice change caused by the Li^+ insertion[29]. The electrochemical conversion mechanism of M_xP_y with Li^+ is commonly considered as[30-32]:

$$M_xP_y + 3yLi^+ + 3ye^- \rightarrow yLi_3P + xM \quad (1)$$

Accordingly, the electrode reaction of Ni_3P may be expressed as follows:

$$Ni_3P + (3-3x)Li \Leftrightarrow (3-3x)Ni + (1-x)Li_3P + xNi_3P_{unreacted} \quad (2)$$

The Ni dispersed among the Ni_3P-Ni can act as the catalyst to facilitate Li_3P decomposition (the converse reaction in Eq. (2)) to improve the electrochemical properties of the Ni_3P-Ni electrode. The material's response to the intensive cycling was examined by XRD and SEM. As shown in Fig. 4f, XRD patterns of Ni_3P-Ni structure before and after being cycled for over 100 cycles are essentially unchanged. SEM micrographs of Ni_3P-Ni array electrode before (Fig. 4g) and after (Fig. 4h) 100 cycles (galvanostatic discharge/charge at a current density of 0.02 mA cm^{-2}) at full charge state confirm a good morphology stability of the Ni_3P-Ni arrays electrode during the lithiation and de-lithiation processes. The morphology stability of the coating can stabilize cycling performance of the electrodes[33]. That is to say, the Ni_3P-Ni arrays anode for lithium-ion battery have a good cycling performance.

Conclusions

In conclusion, advanced Ni_3P-Ni array electrodes were prepared by electroless deposition on 3-D nickel foam successfully. The array structure of Ni_3P-Ni can accommodate volume changes during lithiation/de-lithiation progress and promote high-rate capability. The Ni_3P-Ni arrays exhibit a

promising electrochemical performance as an advanced anode material for LIBs with a specific capacity of 360 mAh g^{-1} at a current density of 0.02 mA cm^{-2} after 100 cycles and good rate capability.

Acknowledgements

This work was supported by the 973 Project of China (No. 2011CB935901), the National Natural Science Foundation of China (Grant No. 51371107) (No. 21203110) (No. 21371108).

References

1. Y. Xu, J. D. Feng, X. C. Chen, K. Kierzek, W. B. Liu, T. Tang and E. Mijowska, Rsc Advances, 2015, 5, 28864-28869.

2. F. Zhang, R. Zhang, J. Feng and Y. Qian, Mater Lett, 2014, 114, 115-118.

3. F. K. Butt, M. Tahir, C. Cao, F. Idrees, R. Ahmed, W. S. Khan, Z. Ali, N. Mahmood, M. Tanveer and A. Mahmood, Acs Appl Mater Interfaces, 2014, 6, 13635-13641.

4. G.-H. Lee, H.-W. Shim and D.-W. Kim, Nano Energy, 2015, 13, 218-225.

5. H. X. Gao, F. Hou, X. R. Zheng, J. C. Liu, A. R. Guo, D. M. Yang and Y. X. Gong, Vacuum, 2015, 112, 1-4.

6. J. P. Tu, X. H. Huang, C. Q. Zhang and J. Y. Xiang, Electrochem Commun, 2007, 9, 1180-1184.

7. J. Xu, H. Thomas, R. W. Francis, K. R. Lum, J. Wang and B. Liang, J Power Sources, 2008, 177, 512-527.

8. D. Silva, O. Crosnier, G. Ouvrard, J. Greedan, A. Safa-Sefat and L. Nazar, Electrochemical and solid-state letters, 2003, 6, A162-A165.

9. M. Cruz, J. Morales, L. Sánchez, J. Santos-Peña and F. Martín, J Power Sources, 2007, 171, 870-878.

10. V. Pralong, D. C. S. Souza, K. T. Leung and L. F. Nazar, Electrochem Commun, 2002, 4, 516-520.

11. H. Pfeiffer, F. Tancret, M.-P. Bichat, L. Monconduit, F. Favier and T. Brousse, Electrochem Commun, 2004, 6, 263-267.

12. F. Gillot, S. Boyanov, L. Dupont, M. L. Doublet, A. Morcrette, L. Monconduit and J. M. Tarascon, Chem Mater, 2005, 17, 6327-6337.

13. R. Alcantara, J. Tirado, J. Jumas, L. Monconduit and J. Olivier-Fourcade, J Power Sources, 2002, 109, 308-312.

14. M. P. Bichat, T. Politova, H. Pfeiffer, F. Tancret, L. Monconduit, J. L. Pascal, T. Brousse and F. Favier, J Power Sources, 2004, 136, 80-87.

15. J. Fullenwarth, A. Darwiche, A. Soares, B. Donnadieu and L. Monconduit, Journal of Materials Chemistry A, 2014, 2, 2050-2059.

16. H. Schlenger, H. Jacobs and R. Juza, Z Anorg Allg Chem, 1971, 385, 177-201.

17. M. Bichat, T. Politova, J. Pascal, F. Favier and L. Monconduit, J Electrochem Soc, 2004, 151, A2074-A2081.

18. M.-P. Bichat, T. Politova, H. Pfeiffer, F. Tancret, L. Monconduit, J.-L. Pascal, T. Brousse and F. Favier, J Power Sources, 2004, 136, 80-87.

19. Z. Zhang, J. Yang, Y. Nuli, B. Wang and J. Xu, Solid State Ionics, 2005, 176, 693-697.

20. D. Souza, V. Pralong, A. Jacobson and L. Nazar, Science, 2002, 296, 2012-2015.

21. J. Liu, Y. Xu, X. Ma, J. Feng, Y. Qian and S. Xiong, Nano Energy, 2014, 7, 52-62.

22. S. Liu, J. Feng, X. Bian, Y. Qian, J. Liu and H. Xu, Nano Energy, 2015, 13, 651-657.

23. S. Liu, X. Bian, J. Liu, C. Yang, X. Zhao, J. Fan, K. Zhang, Y. Bai, H. Xu, Y. Liu and T. Guo, Surface Engineering, 2015, 31, 420-426.

24. A. Araghi and M. H. Paydar, Vacuum, 2013, 89, 67-70.

25. E. Besenyei, B. Zsoldos and O. Geszti, Vacuum, 1983, 33, 35-41.

26. C. Yang, D. Zhang, Y. Zhao, Y. Lu, L. Wang and J. B. Goodenough, J Power Sources, 2011, 196, 10673-10678.

27. F. Gillot, M. Bichat, F. Favier, M. Morcrette, M. Doublet and L. Monconduit, Electrochim Acta, 2004, 49, 2325-2332.

28. Y. Yu, L. Gu, C. Zhu, S. Tsukimoto, P. A. van Aken and J. Maier, Adv Mater, 2010, 22, 2247-2250.

29. K. Zhang, M. B. Katz, B. Li, S. J. Kim, X. Du, X. Hao, J. R. Jokisaari, S. Zhang, G. W. Graham and A. Van der Ven, Adv Mater, 2014, 26, 7365-7370.

30. C. Villevieille, F. Robert, P. L. Taberna, L. Bazin, P. Simon and L. Monconduit, J Mater Chem, 2008, 18, 5956-5960.

31. Y. Lu, J. P. Tu, C. D. Gu, X. L. Wang and S. X. Mao, J Mater Chem, 2011, 21, 17988-17997.

32. Y. Feng, H. Zhang, Y. Mu, W. Li, J. Sun, K. Wu and Y. Wang, Chemistry – A European Journal, 2015, 21, 9229-9235.

33. M. Noh, Y. Kwon, H. Lee, J. Cho, Y. Kim and M. G. Kim, Chem Mater, 2005, 17, 1926-1929.

Fig. 1 (a) XRD patterns of precursor film (electroless deposited Ni-P) with copper foil as substrate (b) XRD patterns and EDX of annealed film (Ni3P-Ni) with copper foil as substrate

Fig. 2 (a) SEM image of uncoated Ni foam. (b) and (c) SEM images of Ni3P-Ni coating on Ni foam substrate. (d) XRD patterns of uncoated Ni foam, electroless deposited Ni-P coated Ni foam and Ni3P-Ni coated Ni foam. (e) SEM image of netlike Ni3P-Ni coated Ni foam. (f) EDX mapping of elemental P corresponding to (e).

Fig. 3 (a) Cyclic voltammogram for Ni3P-Ni arrays from 0.01V to 3 V at rate of 1 mV s-1. (b) The discharge/charge curves and (c) the cycling performance of Ni3P-Ni arrays in the range of 0.01-3 V. (d) Cycling and rate performance of the Ni3P-Ni arrays electrode.

Fig. 4 SEM images of as-deposited Ni3P-Ni arrays (a) and lithiated Ni3P-Ni arrays (b). Schematic of the lithiation for Ni3P-Ni arrays: pristine (c) and lithiated (d). (e) The (231) XRD peak of the Ni3P-Ni film before and after charging with Li+. (f) XRD patterns of Ni3P-Ni structure before and after being cycled for over 100 cycles. SEM images of Ni3P-Ni arrays electrode before (g) and after (h) 100 cycles (galvanostatic discharge/charge at a current density of 0.02 mA cm-2) at full charge state.

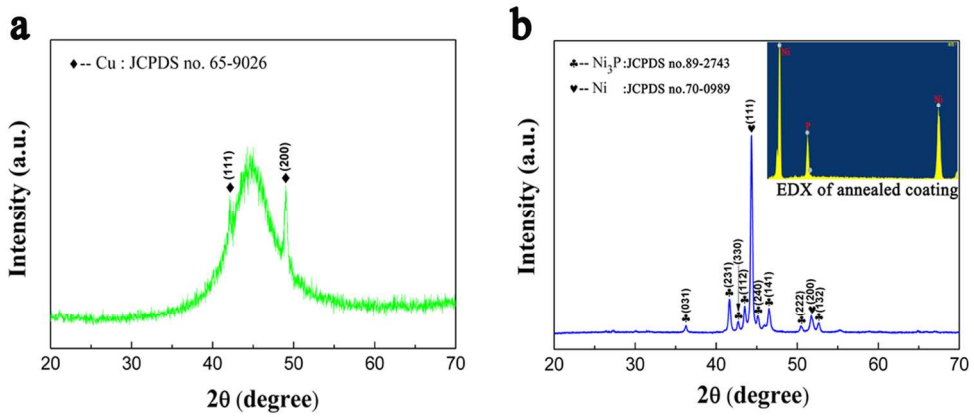

Fig. 1 (a) XRD patterns of precursor film (electroless deposited Ni-P) with copper foil as substrate (b) XRD patterns and EDX of annealed film (Ni3P-Ni) with copper foil as substrate
240x99mm (300 x 300 DPI)

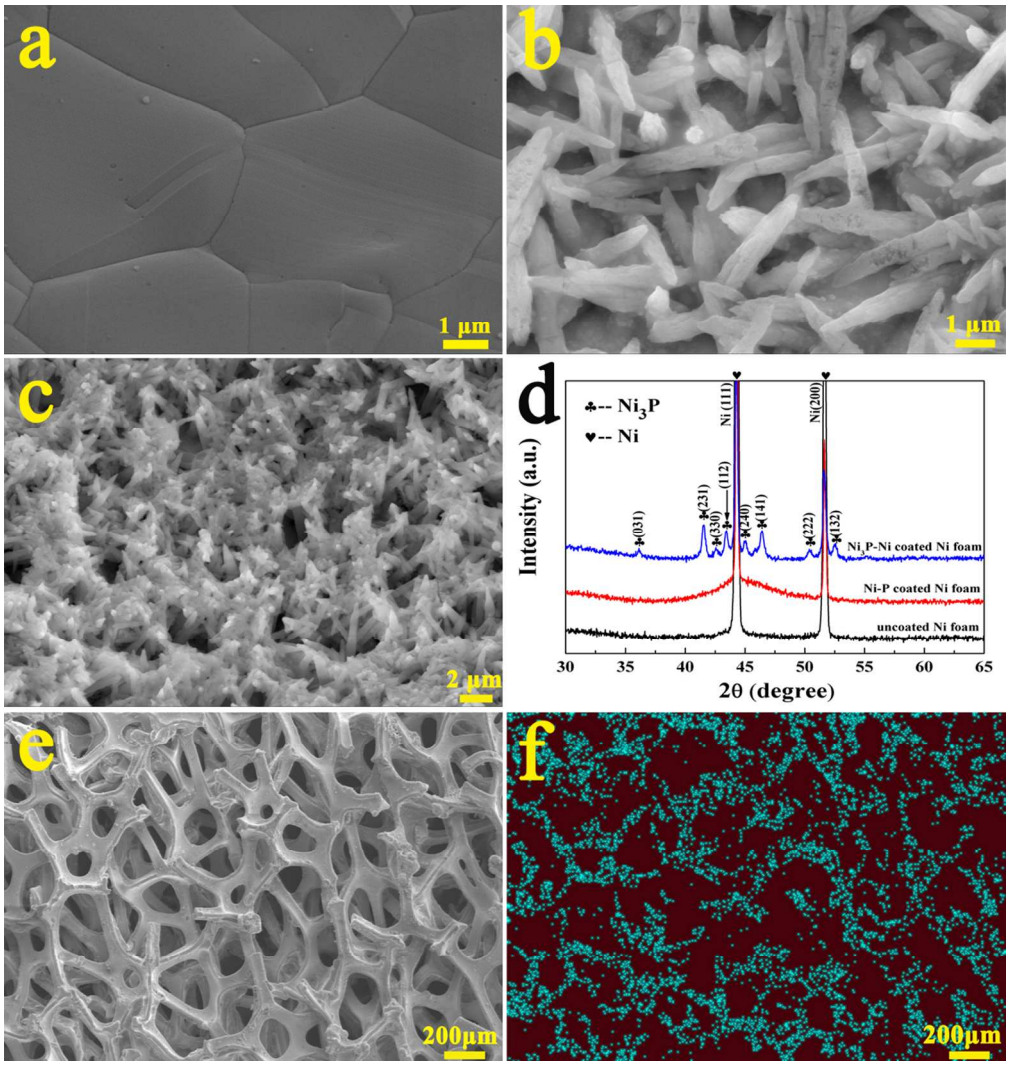

Fig. 2 (a) SEM image of uncoated Ni foam. (b) and (c) SEM images of Ni3P-Ni coating on Ni foam substrate. (d) XRD patterns of uncoated Ni foam, electroless deposited Ni-P coated Ni foam and Ni3P-Ni coated Ni foam. (e) SEM image of netlike Ni3P-Ni coated Ni foam. (f) EDX mapping of elemental P corresponding to (e).
108x114mm (300 x 300 DPI)

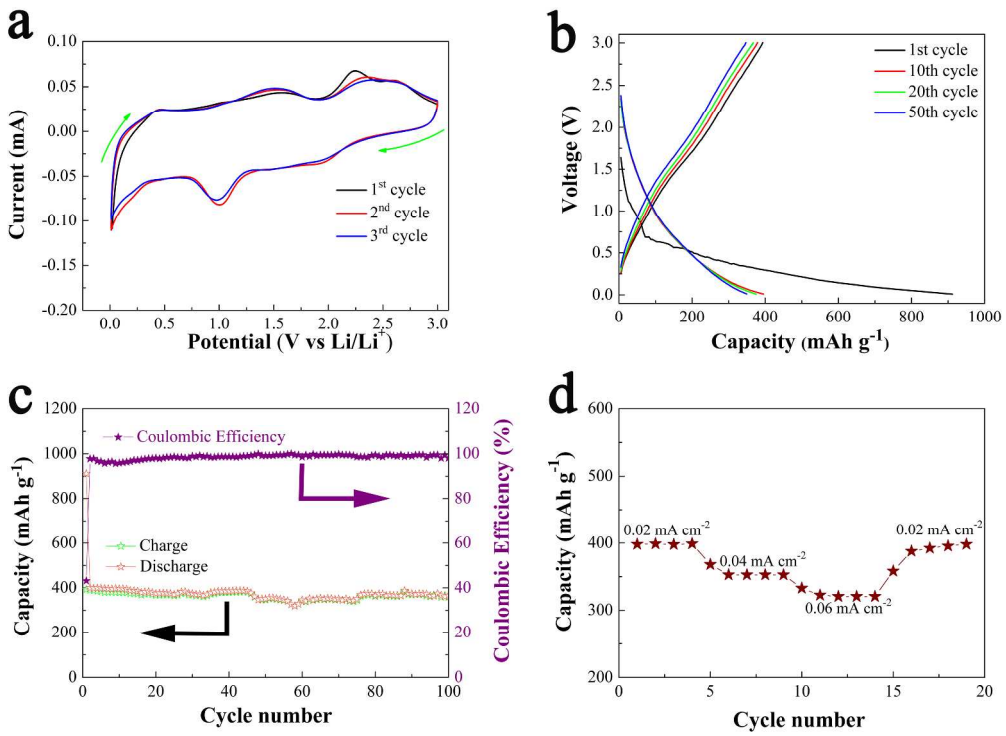

Fig. 3 (a) Cyclic voltammogram for Ni3P-Ni arrays from 0.01V to 3 V at rate of 1 mV s-1. (b) The discharge/charge curves and (c) the cycling performance of Ni3P-Ni arrays in the range of 0.01-3 V. (d) Cycling and rate performance of the Ni3P-Ni arrays electrode.
277x201mm (300 x 300 DPI)

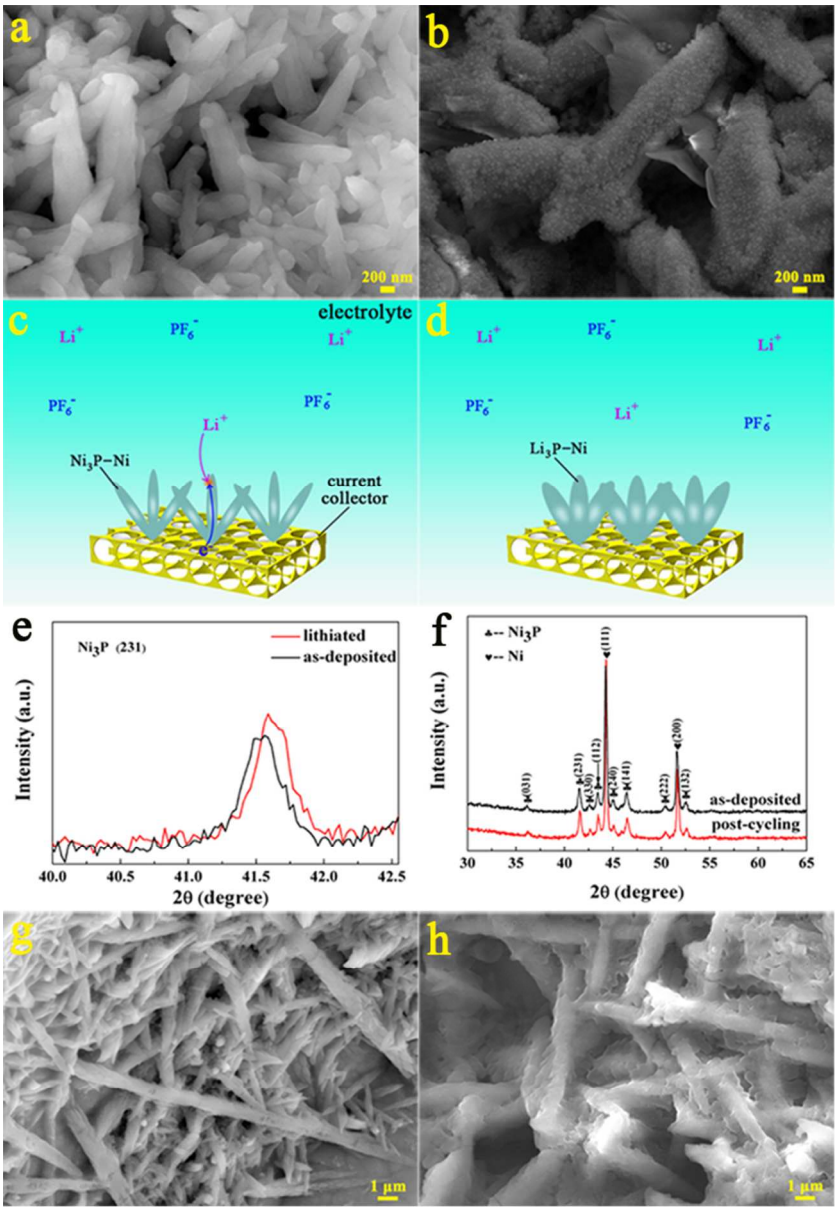

Fig. 4 SEM images of as-deposited Ni3P-Ni arrays (a) and lithiated Ni3P-Ni arrays (b). Schematic of the lithiation for Ni3P-Ni arrays: pristine (c) and lithiated (d). (e) The (231) XRD peak of the Ni3P-Ni film before and after charging with Li+. (f) XRD patterns of Ni3P-Ni structure before and after being cycled for over 100 cycles. SEM images of Ni3P-Ni arrays electrode before (g) and after (h) 100 cycles (galvanostatic discharge/charge at a current density of 0.02 mA cm-2) at full charge state.
82x119mm (300 x 300 DPI)

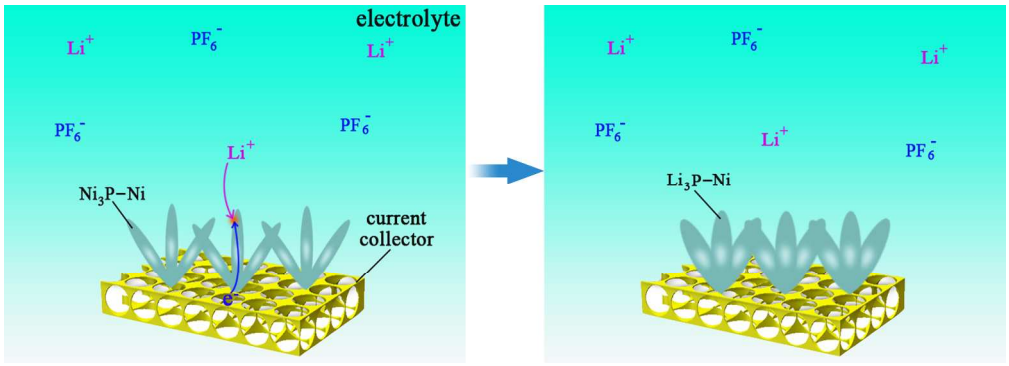

The array structure of Ni3P-Ni can accommodate volume changes during the lithiation/de-lithiation progress and promote high-rate capability because the interspaces in such structure can act as ideal volume expansion buffers.
237x84mm (300 x 300 DPI)